# Lung [$^{18}$F]fluorodeoxyglucose Uptake and Ventilation–Perfusion Mismatch in the Early Stage of Experimental Acute Smoke Inhalation

Guido Musch, M.D., Tilo Winkler, Ph.D., R. Scott Harris, M.D., Marcos F. Vidal Melo, M.D., Ph.D., Tyler J. Wellman, Ph.D., Nicolas de Prost, M.D., Ph.D., Richard L. Kradin, M.D., Jose G. Venegas, Ph.D.

## ABSTRACT

**Background:** Acute lung injury occurs in a third of patients with smoke inhalation injury. Its clinical manifestations usually do not appear until 48–72 h after inhalation. Identifying inflammatory changes that occur in pulmonary parenchyma earlier than that could provide insight into the pathogenesis of smoke-induced acute lung injury. Furthermore, noninvasive measurement of such changes might lead to earlier diagnosis and treatment. Because glucose is the main source of energy for pulmonary inflammatory cells, the authors hypothesized that its pulmonary metabolism is increased shortly after smoke inhalation, when classic manifestations of acute lung injury are not yet expected.

**Methods:** In five sheep, the authors induced unilateral injury with 48 breaths of cotton smoke while the contralateral lung served as control. The authors used positron emission tomography with: (1) [$^{18}$F]fluorodeoxyglucose to measure metabolic activity of pulmonary inflammatory cells; and (2) [$^{13}$N]nitrogen in saline to measure shunt and ventilation–perfusion distributions separately in the smoke-exposed and control lungs.

**Results:** The pulmonary [$^{18}$F]fluorodeoxyglucose uptake rate was increased at 4 h after smoke inhalation (mean ± SD: 0.0031 ± 0.0013 *vs.* 0.0026 ± 0.0010 min$^{-1}$; $P < 0.05$) mainly as a result of increased glucose phosphorylation. At this stage, there was no worsening in lung aeration or shunt. However, there was a shift of perfusion toward units with lower ventilation-to-perfusion ratio (mean ratio ± SD: 0.82 ± 0.10 *vs.* 1.12 ± 0.02; $P < 0.05$) and increased heterogeneity of the ventilation–perfusion distribution (mean ± SD: 0.21 ± 0.07 *vs.* 0.13 ± 0.01; $P < 0$ .05).

**Conclusion:** Using noninvasive imaging, the authors demonstrated that increased pulmonary [$^{18}$F]fluorodeoxyglucose uptake and ventilation–perfusion mismatch occur early after smoke inhalation. **(Anesthesiology 2014; 120:683-93)**

SMOKE inhalation injury is present in 20–30% of patients admitted to burn centers.[1–3] Isolated inhalation injury has a mortality rate of approximately 10%,[4] and smoke inhalation increases the odds of mortality in burn patients by more than twofold.[5,6] Anesthesiologists are crucial providers of early care for these patients both because they are frequently called to secure the airway and initiate mechanical ventilation and because they provide general anesthesia for excision and grafting procedures.

Initial clinical manifestations of smoke inhalation usually result from large airway epithelial injury. They consist of mucosal hyperemia, edema and ulceration, cast formation, and bronchial obstruction. These are usually diagnosed and treated by bronchoscopy.[3,7] However, approximately one third of patients with inhalation injury develop acute lung injury (ALI) over the days after smoke exposure.[7,8] This pulmonary response to smoke inhalation is characterized by an inflammatory process and manifests clinically with decreased $Pa_{O_2}/F_{I_{O_2}}$,[8] decreased respiratory compliance,[9] and a need for mechanical ventilation.[3,10] Because these clinical manifestations of ALI typically appear up to 72 h after smoke exposure,[3] the need for

### What We Already Know about This Topic

- Smoke inhalation injury involves pulmonary inflammation, which does not become clinically apparent for 2–3 days after exposure
- A noninvasive method for earlier identification of pulmonary inflammatory processes could aid in better understanding of the mechanisms of lung injury

### What This Article Tells Us That Is New

- In sheep undergoing mild smoke exposure to one lung, [$^{18}$F]-fluorodeoxyglucose uptake, as measured by positron emission tomography, increased in the exposed lung 4 h after exposure, before worsening shunt or aeration

This article is featured in "This Month in Anesthesiology," page 1A. This work was presented, in part, at the International Conference of the American Thoracic Society in New Orleans, Louisiana, May 19, 2010.

Submitted for publication March 1, 2013. Accepted for publication August 12, 2013. From the Department of Anesthesia, Critical Care, and Pain Medicine (G.M., T.W., M.F.V.M., T.J.W., N.d.P., J.G.V.), Department of Medicine, Pulmonary and Critical Care Unit (R.S.H.), and Department of Pathology (R.L.K.), Massachusetts General Hospital and Harvard Medical School, Boston, Massachusetts.

earlier identification of smoke inhalation–induced ALI has been recognized.[1] Whether such identification is possible depends on when inflammatory changes in lung parenchyma start and on whether such changes can be measured noninvasively.

An experimental study demonstrated that lung lymph flow is increased at 4 h after smoke inhalation,[11] suggesting that initial signs of pulmonary inflammation may appear earlier than the increase in shunt fraction,[12] decrease in $Pa_{O_2}/F_{I_{O_2}}$,[12,13] neutrophil infiltration,[14] and activation of inflammatory pathways[15] that occur in the lungs of animals at 24–48 h after smoke inhalation. Increased uptake of glucose by pulmonary inflammatory cells is also a sign of inflammation.[16] In fact, positron emission tomography (PET) imaging of [$^{18}$F]fluorodeoxyglucose ([$^{18}$F]FDG) uptake has been used to noninvasively quantify the pulmonary inflammatory response to insults such as endotoxin,[17,18] mechanical ventilation,[19–21] and chemical[22] and microbial[23] agents. We previously showed that intense cigarette smoking increases pulmonary [$^{18}$F]FDG uptake.[24] We also showed, in a large animal model of ventilator-induced lung injury, that [$^{18}$F]FDG uptake was increased after only 90 min of mechanical ventilation,[19] suggesting that increased [$^{18}$F]FDG uptake is an early sign of lung inflammation. These observations led us to ask the question of whether pulmonary [$^{18}$F]FDG uptake is increased at an early stage after acute smoke inhalation. Answering this question could provide new insight into the pathophysiology of smoke inhalation–induced ALI and lead to methods for earlier diagnosis and possible treatment of this complication.

In this study, we used molecular imaging with PET and tracer kinetic modeling in a sheep model of acute smoke inhalation to assess whether an increase in pulmonary [$^{18}$F]FDG uptake occurred at a stage in which deterioration of gas exchange was not yet expected.[12,13] To minimize the number of animals, we exposed only one lung to the inhalation injury while the contralateral lung was used as control.[24,25] We used dynamic PET imaging of intravenously infused [$^{13}$N]nitrogen ($^{13}N_2$) in saline to measure shunt fraction and the ventilation–perfusion distribution separately in the smoke-exposed and control lungs.

## Materials and Methods

### Experimental Protocol

The experimental procedures were approved by the Subcommittee on Research Animal Care of the Massachusetts General Hospital, Boston, Massachusetts. Care and handling of animals were in accordance with the guidelines of the National Institutes of Health, Bethesda, Maryland. After fasting overnight, five sheep weighing 25.8 ± 3.7 kg (mean ± SD) were premedicated (intramuscular midazolam 1 mg/kg and ketamine 4 mg/kg), anesthetized (intravenous propofol 5 mg/kg followed by 150–200 $\mu g \cdot kg^{-1} \cdot min^{-1}$ and fentanyl 10–30 $\mu g \cdot kg^{-1} \cdot h^{-1}$), intubated through a tracheotomy, and mechanically ventilated (tidal volume, 11 ml/kg; rate, 14–16 breaths/min; $F_{I_{O_2}}$, 0.5). Using aseptic surgical technique, a catheter was inserted in the femoral artery and a Swan–Ganz catheter (model 831HF75; Edwards Lifesciences, Irvine, CA) in the jugular vein. The endotracheal tube was then substituted with a left-sided double lumen endobronchial tube modified to allow aeration of the right upper lobe.[19,26] Proper position of the tube was confirmed by fiberoptic bronchoscopy and isolation by inflating each lung separately while watching for bubbles in a water seal system connected to the contralateral lung. The sheep were then turned and kept prone in a cradle for the remainder of the study. The rationale for the use of the prone position was to favor homogeneous lung expansion, minimize atelectasis, and promote uniform distribution of the inhaled smoke.

Forty-eight breaths of cotton smoke in room air were delivered to the left lung while the other lung was kept at $F_{I_{O_2}}$ 0.5 (fig. 1). We used a smoking apparatus similar to that in the study by Ballard-Croft *et al.*[27] A modified bee smoker was connected to the gas inlet of the bellows controlled by an Ohmeda anesthesia ventilator (Ohmeda 7000, Datex-Ohmeda, Madison, WI) with long tubing to allow for cooling of the smoke. The gas outlet was connected to the endobronchial lumen of the double-lumen tube. Because the Ohmeda ventilator controlled the deflation of the bellows, this system allowed maintenance of constant respiratory rate and tidal volume during induction of the inhalation injury.[27,28] Tidal volume to the smoke-exposed lung was set to achieve the same end-inspiratory pressure as during previous bilateral ventilation to prevent disruption of the ventilatory pattern.

The double-lumen tube was then substituted with an endotracheal tube through which mechanical ventilation was resumed at previous settings. $F_{I_{O_2}}$ was kept at 0.5 for the remainder of the study. Arterial carboxyhemoglobin was 14.1 ± 4.4% 10 min after smoke exposure (OSM-3 Co-oximeter; Radiometer Medical, Copenhagen, Denmark).

The sheep were transported prone to the PET suite. Starting at 3.5 h after smoke inhalation, a 10-min PET transmission scan was acquired to measure lung aeration, followed by a 4-min $^{13}N_2$-saline bolus infusion scan to measure shunt and ventilation–perfusion distributions and a 45-min [$^{18}$F]FDG scan to measure metabolic activity. At the end of imaging, the animals were deeply anesthetized (with propofol 10 mg/kg and fentanyl 25 μg/kg), euthanized (with intravenous potassium 40 mM), and the lungs were excised.

### PET Imaging

The PET scanner imaged 15 contiguous 6.5-mm thick transverse slices, corresponding to approximately 70% of the sheep lung,[29] at a spatial resolution of 6.5-mm full width at half maximum (PC-4096; Scanditronix AB, Uppsala,

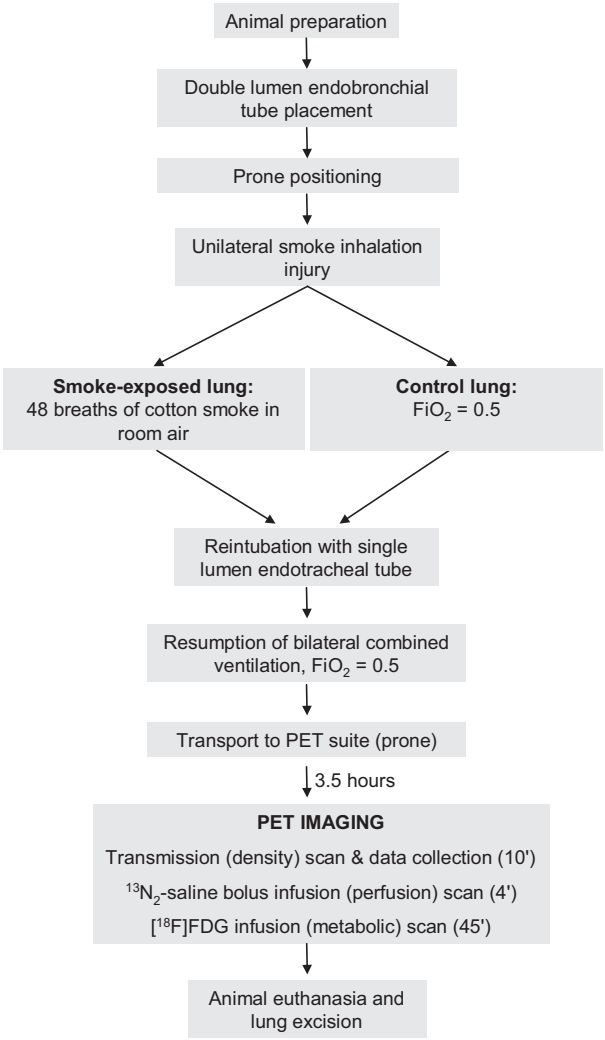


**Fig. 1.** Protocol schema. [$^{18}$F]FDG = [$^{18}$F]fluorodeoxyglucose; $F_{IO_2}$ = inspiratory oxygen fraction; $^{13}N_2$ = [$^{13}$N]nitrogen; PET = positron emission tomography.

Sweden). Emission scans were reconstructed with a filtered back projection algorithm and low pass filtered to an effective in-plane spatial resolution of $13 \times 13\,mm^2$. Three types of scans were acquired:

**Transmission (Density) Scan.** Transmission (density) scan was performed to calculate gas fraction, correct emission scans for tissue attenuation, and demarcate the lung field.[19]

**$^{13}N_2$-Saline Bolus Infusion (Perfusion) Scan.** $^{13}N_2$ (34 ± 6 mCi) dissolved in saline solution (35–40 ml) was infused in the jugular vein as a bolus over the initial 3 s of a 60-s apnea performed at mean airway pressure.[30] Intravenous pancuronium (0.1 mg/kg) was administered before $^{13}N_2$-saline imaging to ensure apnea. Sequential PET frames ($8 \times 2.5$ s, $10 \times 10$ s, $4 \times 30$ s) were taken to measure $^{13}N_2$ kinetics during apnea and the ensuing 3 min of $^{13}N_2$ washout by breathing after resumption of mechanical ventilation. Because of the low solubility of nitrogen in blood (partition coefficient water-to-air is 0.015 at 37°C), upon arrival into pulmonary capillaries virtually all $^{13}N_2$ diffuses at first pass into the alveolar airspace of perfused and aerated regions, where it accumulates in proportion to regional perfusion for the remainder of apnea. In contrast, in regions that contain shunting alveolar units, $^{13}N_2$ kinetics during apnea show a peak of tracer concentration in the early PET frames, corresponding to arrival of the bolus of tracer with pulmonary blood flow, followed by an exponential decrease toward a plateau. This decrease is related to the magnitude of regional shunt because $^{13}N_2$ is not retained in shunting units during apnea. Shunt fractions of the smoke-exposed and control lungs were calculated with a model applied to $^{13}N_2$ apnea kinetics.[31]

**Computation of Ventilation-to-Perfusion Ratio Distribution.** When breathing is resumed, $^{13}N_2$ that accumulated in the alveolar airspace during apnea is excreted by ventilation. Accordingly, the $^{13}N_2$ washout kinetics after resumption of breathing were used to compute specific ventilation and ventilation-to-perfusion ratios at the voxel level as previously described.[29,32] The equations and calculations that were implemented to compute ventilation–perfusion distributions are reported in the appendix.

To account for possible intravoxel ventilation–perfusion heterogeneity in the computation of total heterogeneity, each voxel was classified as composed of either a single-ventilating compartment, when the semilogarithmic activity–time washout plot was linear, or two compartments, when the plot was not linear. Specific alveolar ventilation (*i.e.*, alveolar ventilation per unit of gas volume) was calculated as the reciprocal of the time constant(s) of the $^{13}N_2$ washout curve. For one-compartment voxels, the $^{13}N_2$ activity at the end of apnea was taken as proportional to perfusion to aerated units in the voxel. For two-compartment voxels, perfusion to the slow ventilating compartment was obtained by extrapolating the last 90 s of $^{13}N_2$ washout back to the end of apnea and perfusion to the fast compartment by subtracting that of the slow compartment from end-apnea activity.[29]

Specific ventilation-to-perfusion ratios were calculated for each compartment of each voxel and normalized by their perfusion-weighted mean calculated over both lungs. Their logarithm was plotted against the corresponding fraction of perfusion in separate distribution histograms for the smoke-exposed and control lungs. Ventilation–perfusion heterogeneity was computed as the SD of the perfusion-weighted logarithmic distribution.

**[$^{18}$F]FDG Infusion (Metabolic Activity) Scan.** After $^{13}N_2$ clearance, [$^{18}$F]FDG (5–10 mCi) was infused in the jugular vein over 60 s. Sequential PET frames ($9 \times 10$ s, $4 \times 15$ s, $1 \times 30$ s, $7 \times 60$ s, $15 \times 120$ s, $1 \times 300$ s) were acquired over 45 min to measure pulmonary [$^{18}$F]FDG kinetics. Pulmonary arterial blood samples (1 ml) were drawn at 5.5, 9.5, 25, 37, and 42.5 min, spun down, and the activity of plasma was measured in a γ counter cross-calibrated with the PET scanner. Plasma activity was used to obtain an image-derived input function from a region defined on the

blood pool of the right heart for [$^{18}$F]FDG compartmental modeling.[33]

After being transported into the cell by the same mechanism as glucose, [$^{18}$F]FDG is phosphorylated by hexokinase to [$^{18}$F]FDG-6-phosphate, which accumulates in proportion to the metabolic rate of the cell. Sokoloff's three-compartment model[34,35] was used to estimate the blood-to-tissue [$^{18}$F]FDG transport rate ($k_1$), the rate for reverse transport ($k_2$), and the rate of phosphorylation ($k_3$). These individual rate constants were used to compute the [$^{18}$F]FDG net uptake rate:[35]

$$Ki = \frac{k_1 \cdot k_3}{(k_2 + k_3)} \quad (1)$$

Ki represents glucose metabolic activity per unit volume of lung and is therefore independent of lung size.

The fractional distribution volume of the [$^{18}$F]FDG-6-phosphate precursor pool was calculated as:[34]

$$F_e = \frac{k_1}{(k_2 + k_3)} \quad (2)$$

The [$^{18}$F]FDG-6-phosphate precursor pool represents the [$^{18}$F]FDG pool available for phosphorylation by hexokinase (*i.e.*, intracellular hexokinase-accessible [$^{18}$F]FDG). Consequently, $F_e$ is a measure of substrate availability for phosphorylation.

From equations 1 and 2, it follows that:

$$Ki = F_e \cdot k_3 \quad (3)$$

**Selection of Voxels for Analysis.** Aerated lung regions were identified by applying a threshold to the transmission scan. Perfused regions, including regions that were perfused but not aerated (*i.e.*, shunting), were identified by applying an activity threshold to frames 3 through 8 of the $^{13}N_2$-saline perfusion scan (*i.e.*, 5–20 s after the start of $^{13}N_2$-saline infusion). A lung field mask was created, for each lung of each animal, from the union of aerated regions and perfused regions and was refined by hand to exclude main bronchi and large pulmonary vessels.

A region of interest corresponding to the blood pool of the right heart and pulmonary artery was defined by applying an activity threshold to the first two frames of the $^{13}N_2$-saline scan. During this time (<5 s since start of injection), virtually all $^{13}N_2$ is confined to the right heart cavity and pulmonary artery. This region of interest was then applied to the [$^{18}$F]FDG scan to obtain the input function for [$^{18}$F]FDG compartmental modeling.[33]

### Histologic Analysis

At the end of the study protocol, the lungs were excised, fixed with Trump fixative (4% formaldehyde and 1% glutaraldehyde in phosphate-buffered saline) for 7 days at 4°C, and processed as previously described.[19] After fixation, the lungs were cut in 1-cm thick sagittal slices. By using a stratified random sampling technique, a 1-cm$^3$ block of lung tissue was selected from each of the ventral, middle, and dorsal regions of the second most lateral slice of each lung. The tissue block was embedded in paraffin, and 5-μm thick sections were cut, mounted, and stained with hematoxylin and eosin for light microscopy. Neutrophils were counted in 10 high-power (×400 magnification) fields (0.26 mm$^2$ per field) per block (*i.e.*, 30 fields per lung) by an expert pathologist (R.L.K.) who was blinded as to whether the lung was exposed to cotton smoke or not. The total number of counted neutrophils per lung is reported.

### Statistical Analysis

Differences between the smoke-exposed and control lungs were tested with the nonparametric Sign test[36] because of the small sample size. Furthermore, differences that resulted significant ($P < 0.05$) were also tested with two-tailed Student paired *t* test (Microsoft Excel 2003; Microsoft Corp., Redmond, WA). To be conservative, only differences significant with both tests are reported. Data are presented as mean ± SD.

## Results

Physiologic data collected during the last 2 min of the transmission scan are shown in table 1. A PET image showing higher [$^{18}$F]FDG activity in the smoke-exposed than in the control lung is shown in figure 2. Ki was significantly higher in the smoke-exposed than in the control lung ($0.0031 \pm 0.0013$ *vs.* $0.0026 \pm 0.0010$ min$^{-1}$; $P < 0.05$), whereas neither shunt fraction nor gas fraction was different between the two lungs (fig. 3). The increase in Ki in the smoke-exposed lung was associated with an increase in the rate of [$^{18}$F]FDG phosphorylation (*i.e.*, $k_3$) in four of the five sheep (table 2). In the fifth sheep, the increase in Ki was instead driven by an increase in $F_e$, which represents the distribution volume of [$^{18}$F]FDG available for phosphorylation. Consistent with this finding was the finding that this sheep showed higher lung density (*i.e.*, lower gas fraction) in the smoke-exposed than in the control lung. The difference in $F_e$ between the smoke-exposed and control lungs was indeed strongly inversely correlated with that in gas fraction: $\Delta Fgas = -2.64 \cdot \Delta F_e - 0.01$ ($r = 0.88$; $P < 0.05$).

Despite the fact that shunt fraction had not yet increased in the smoke-exposed lung, the perfusion-weighted ventilation–perfusion distribution showed significant differences between the two lungs (fig. 4). In the smoke-exposed lung, this distribution was systematically shifted toward lower ventilation-to-perfusion ratios. Accordingly, the mean of the distribution was lower in the smoke-exposed than in the control lung ($0.82 \pm 0.10$ *vs.* $1.12 \pm 0.02$; $P < 0.05$). Furthermore, the SD of the distribution was higher in the

**Table 1.** Physiologic Variables at End of Transmission Scan

| Variable | Value |
|---|---|
| TV, ml/kg | 10.9 ± 2.0 |
| RR, breaths/min | 15.4 ± 1.5 |
| Paw, cm $H_2O$ | 15.8 ± 3.6 |
| $PaCO_2$, mmHg | 35 ± 5 |
| pHa | 7.48 ± 0.06 |
| $PaO_2$, mmHg | 228 ± 41 |
| $PvCO_2$, mmHg | 37 ± 4 |
| pHv | 7.46 ± 0.06 |
| $PvO_2$, mmHg | 68 ± 7 |
| CO, l/min | 8.4 ± 0.9 |
| HR, beats/min | 170 ± 14 |
| SAP, mmHg | 125 ± 13 |
| DAP, mmHg | 78 ± 14 |
| MAP, mmHg | 100 ± 12 |
| SPAP, mmHg | 26 ± 5 |
| DPAP, mmHg | 11 ± 6 |
| MPAP, mmHg | 18 ± 5 |
| PAOP, mmHg | 6 ± 3 |
| T, °C | 38.5 ± 1.2 |

Values are presented as mean ± SD.

CO = cardiac output; DAP = diastolic arterial pressure; DPAP = diastolic pulmonary arterial pressure; HR = heart rate; MAP = mean arterial pressure; MPAP = mean pulmonary arterial pressure; $PaCO_2$ = arterial carbon dioxide tension; $PaO_2$ = arterial oxygen tension (at $FIO_2$ 0.5); PAOP = pulmonary arterial occlusion pressure; Paw = end-inspiratory airway pressure; pHa = arterial pH; pHv = mixed venous pH; $PvCO_2$ = mixed venous carbon dioxide tension; $PvO_2$ = mixed venous oxygen tension; RR = respiratory rate; SAP = systolic arterial pressure; SPAP = systolic pulmonary arterial pressure; T = body temperature; TV = tidal volume.

smoke-exposed than in the control lung (0.21 ± 0.07 *vs.* 0.13 ± 0.01; $P < 0.05$).

Pulmonary neutrophil count tended to be higher in the smoke-exposed than in the control lung (513 ± 138 *vs.* 481 ± 166 neutrophils per 7.8 $mm^2$), but this difference was not significant because one sheep (s4) had lower neutrophil count in the smoke-exposed (497) than in the control (528) lung. Observation of the slides revealed a patchy distribution of the smoke-induced histological injury. Histological abnormalities characteristic of early ALI such as capillary engorgement, alveolar wall thickening, and erythrocyte extravasation were interspersed among relatively preserved parenchyma (fig. 5).

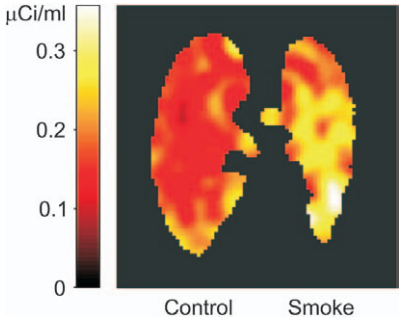


**Fig. 2.** Positron emission tomography image representing the time-averaged pulmonary [$^{18}$F]fluorodeoxyglucose activity between 27 and 45 min since injection, 4 h after unilateral cotton smoke inhalation to the left lung of sheep s2. Note higher activity in the smoke-exposed than in the control lung.

## Discussion

The main results of this study are (1) the pulmonary [$^{18}$F]FDG net uptake rate was increased after acute cotton smoke inhalation; (2) this increase occurred by 4 h after injury and was mainly due to an increased phosphorylation by hexokinase; and (3) although at this early stage there was no decrease in lung aeration or increase in shunt fraction, the perfusion-weighted ventilation–perfusion distribution was more heterogeneous and shifted toward units with lower ventilation-to-perfusion ratio compared with the control lung.

### *Rationale of the Model and Critique of the Experiment*

In line with previous investigations,[11–13] we used a pure smoke inhalation injury model, because we wanted to investigate the metabolic response to a direct pulmonary insult. We recognize that many patients with smoke inhalation injury also have skin burn, which has been shown to lead to lung injury[37] and to augment the pulmonary inflammatory effect of smoke inhalation.[38] Consequently, concomitant skin burn is expected to further magnify the increase in [$^{18}$F]FDG uptake that we observed after smoke inhalation alone.

Previous studies in ALI models have consistently shown that the increase in pulmonary [$^{18}$F]FDG uptake above the baseline metabolic rate of the lung is mainly attributable to activated neutrophils.[17,19,22,23] However, other cell types activated by the inflammatory response also contribute to this signal, including monocytes,[39] eosinophils,[40] endothelial cells,[41] and type 2 pneumocytes.[42] Therefore, [$^{18}$F]FDG uptake is considered a measurement of the overall pulmonary metabolic inflammatory response.[43]

This less than absolute specificity of the [$^{18}$F]FDG signal for neutrophils could be one of the explanations for the lack of a significant difference in lung neutrophil count between the smoke-exposed and control lungs despite a significant increase in Ki. It is worth noting, though, that this lack was due to a single sheep having higher neutrophil count in the control lung. Despite this, there was a positive trend between Ki and neutrophil count ($r = 0.38$, nonsignificant), which is remarkable given the difference in sampling volume and the topographical heterogeneity in the distribution of the histological injury (fig. 5). In fact, whereas the measurement of Ki reflects the average [$^{18}$F]FDG uptake rate over approximately 70% of the lung, neutrophils were counted over a minuscule fraction of lung (7.8 $mm^2$). A second explanation might be that at early stages of injury, Ki reflects more the activation status than the number of these cells.

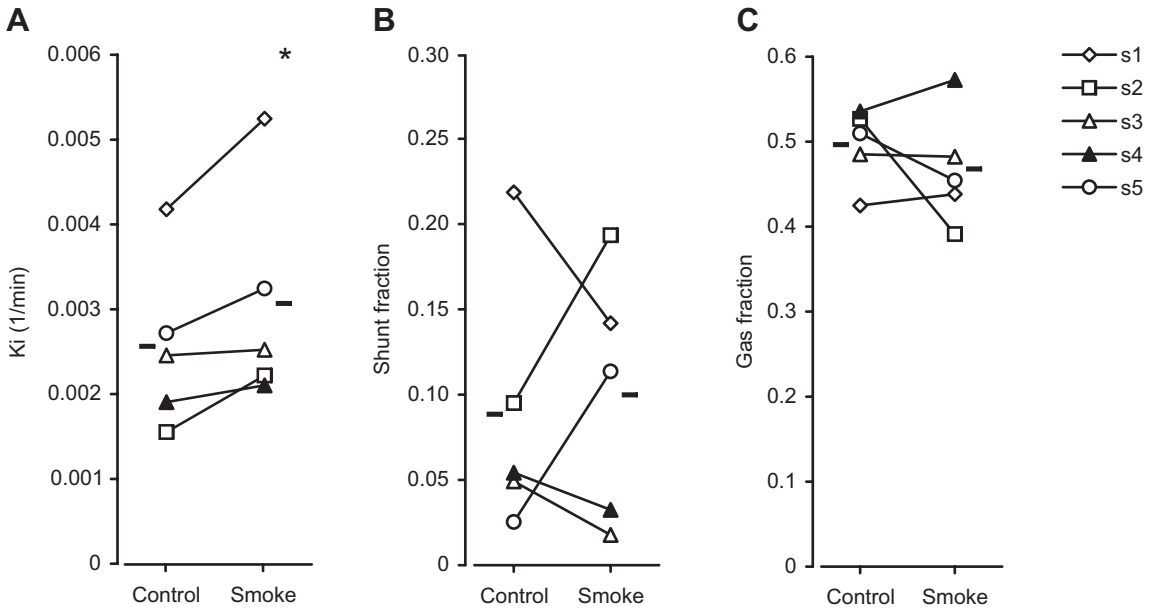


**Fig. 3.** (*A*) [$^{18}$F]fluorodeoxyglucose net uptake rate (Ki), (*B*) shunt fraction, and (*C*) gas fraction after unilateral cotton smoke inhalation in five sheep (s1 through s5). *Horizontal dashes* indicate means. Note the systematic increase in Ki of the smoke-exposed lung. *$P < 0.05$ smoke-exposed *versus* control lung.

### *Pulmonary [$^{18}$F]FDG Uptake and Ventilation–Perfusion Mismatch in the Early Stage of Smoke Inhalation Injury*

Approximately one third of patients with smoke inhalation injury develop ALI.[7] In these patients, clinical manifestations of ALI such as hypoxemia and abnormal chest radiograph tend to develop between 24 and 72 h after smoke exposure.[1,3,7,8] The need to identify pulmonary inflammatory changes that occur earlier than that has been highlighted as an area in need of investigation.[1] Recently, Oh *et al.*[44] showed that the presence of abnormalities on lung computed tomography, such as increased interstitial markings, ground glass opacification, and consolidation, within the first 24 h since admission to a burn center was associated with an increased odds ratio for subsequent development of clinical ALI. In this study, we demonstrated that an increase in pulmonary [$^{18}$F]FDG uptake was already present at 4 h after smoke inhalation. The advantage of this PET method, compared with computed tomography, is that it measures biochemical processes induced by inflammation that are expected to precede the structural changes apparent on computed tomography. Furthermore, by applying compartmental modeling to the tracer kinetic data, we could identify biochemical steps of glucose metabolism responsible for increased metabolic activity: Analysis of the parameters $k_3$ and Fe (table 2) shows that this increase was due to greater phosphorylative activity ($k_3$ is directly related to hexokinase activity)[45] and/or increased availability of [$^{18}$F]FDG for phosphorylation. The advantage of dynamic imaging with compartmental modeling is that it can quantify those steps of glucose metabolism *in vivo* noninvasively. In the setting of smoke inhalation–induced ALI, we speculate that this approach might be valuable to tailor the clinical translation of promising antiinflammatory therapies that carry a risk of toxicity or morbidity only to patients with the highest levels of inflammatory metabolic activity and to follow the efficacy of such therapies over time, similar to the proposed use of $k_3$ for early monitoring of the efficacy of chemohormonotherapy in breast cancer.[46] Examples of such therapies include compound C, which inhibits adenosine monophosphate-activated protein kinase,[47,48] and selective bronchial artery administration

**Table 2.** Parametric Determinants of the Increase in Pulmonary [18F]fluorodeoxyglucose Net Uptake Rate (Ki) of the Smoke-exposed Lung

| | $k_3$ (min$^{-1}$) | | $F_e$ | |
|---|---|---|---|---|
| Sheep No. | Control | Smoke | Control | Smoke |
| Sheep s1 | 0.019 | 0.025 | 0.214 | 0.213 |
| Sheep s2 | 0.010 | 0.012 | 0.157 | 0.188 |
| Sheep s3 | 0.036 | 0.046 | 0.068 | 0.055 |
| Sheep s4 | 0.020 | 0.024 | 0.097 | 0.086 |
| Sheep s5 | 0.024 | 0.022 | 0.115 | 0.146 |
| Mean | 0.022 | 0.026 | 0.130 | 0.138 |
| SD | 0.009 | 0.013 | 0.057 | 0.067 |

$F_e$ is the distribution volume of the [$^{18}$F]fluorodeoxyglucose ([$^{18}$]FDG)-6-phosphate precursor pool, expressed as a fraction of lung volume; $k_3$ is the rate of phosphorylation of [$^{18}$F]FDG to [$^{18}$F]FDG-6-phosphate by hexokinase. The [$^{18}$F]FDG net uptake rate is $Ki = F_e \cdot k_3$. The increase in Ki in the smoke-exposed lung (fig. 3A) was associated with an increase in $k_3$ in sheep s1 through s4, indicating an increased phosphorylation of [$^{18}$F]FDG by hexokinase. In sheep s5, the determinant of the Ki increase was an increase in $F_e$.

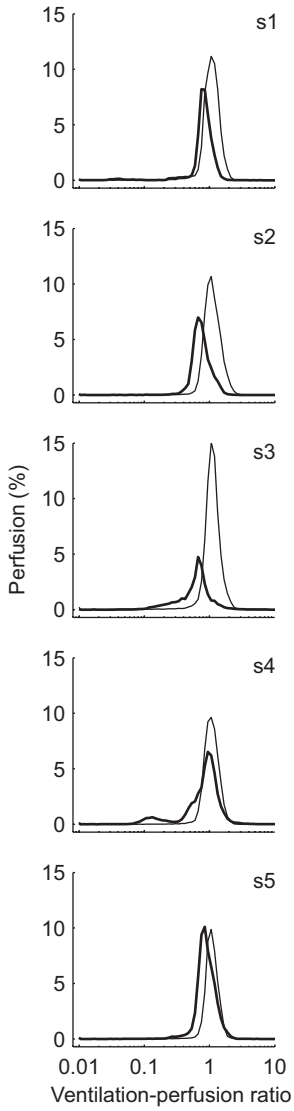


**Fig. 4.** Perfusion-weighted mean-normalized ventilation–perfusion distributions of ventilated alveolar units in the smoke-exposed (*bold line*) and control (*thin line*) lungs, derived by positron emission tomography imaging of infused [$^{13}$N]nitrogen washout kinetics. Note systematic shift of the distribution to the left in the smoke-exposed lung.

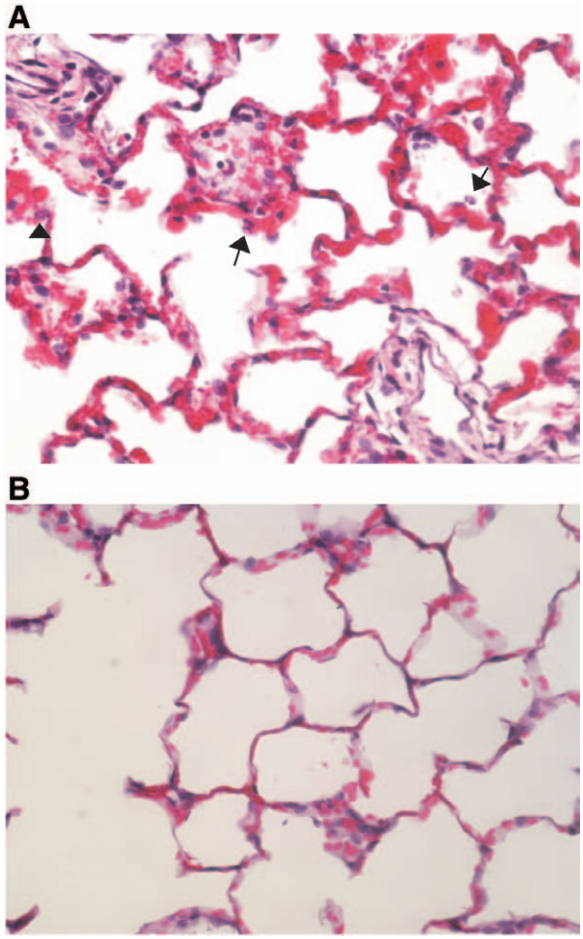


**Fig. 5.** (*A*) Histological changes characteristic of early acute lung injury such as alveolar wall thickening and capillary engorgement are present with a patchy distribution in the smoke-exposed lung. Intraalveolar (*arrows*) and interstitial (*arrowhead*) neutrophils can be identified. (*B*) The control lung, instead, appears largely normal. Hematoxylin and eosin staining.

of reactive nitrogen species decomposition catalysts[49] or poly(ADP-ribose) polymerase inhibitors.[50]

The increase in Ki in the smoke-exposed lung averaged 20%. The magnitude of this increase may have been small because the degree of injury, as gauged by the carboxyhemoglobin level and histology (fig. 5), was mild. A carboxyhemoglobin of 14% should correspond to approximately 30% in a bilateral injury model. This is substantially lower than that of other experimental studies of smoke-induced ALI, which reported levels greater than 50%.[51] The relative magnitude of the Ki increase, however, is similar to that we found in most animals in which lungs were injuriously ventilated with end-inspiratory pressure of 50 cm $H_2O$ and end-expiratory pressure of 10 cm $H_2O$.[19] Although we recognize that the distribution of the data in figure 3A would not allow identification of a threshold of [$^{18}$F]FDG uptake above which smoke-induced ALI could be identified, we emphasize that identifying such threshold was not a goal of this experimental work. Our goal was to assess whether there was an increase of [$^{18}$F]FDG uptake at a very early stage of injury. A receiver-operating characteristic analysis of the ability of [$^{18}$F]FDG uptake to discriminate between subjects that will or will not develop ALI after smoke inhalation would seem more suited for a pilot clinical study that builds on the effect demonstrated in this experiment. Such a study could select patients most at risk of developing ALI according to other criteria, such as carboxyhemoglobin level and bronchoscopic findings, to determine if PET adds value, similarly to what has been done with computed tomography.[44]

Chemical irritants in smoke trigger the production of inflammatory mediators in the bronchial epithelium, such as nitric oxide,[52] peroxynitrite,[53] and interleukin-8.[54] These

mediators reach the lung through the bronchial circulation, triggering pulmonary inflammation, dysfunction,[55] and recruiting neutrophils, which play an important role in the pathogenesis of smoke inhalation injury.[56,57] Our results indicate that progression of this inflammatory process from the airway to the pulmonary parenchyma with ensuing cell metabolic activation and associated ventilation–perfusion mismatch occurs earlier than it would be inferred from previous studies showing that 24–48 h were needed to observe reduced $Pa_{O_2}/F_{IO_2}$,[12,13] neutrophil infiltration,[14] and nuclear factor kappa-B activation[15] in bronchioles and pulmonary parenchyma. This finding is important because it implies that the therapeutic window for antiinflammatory therapies[10,58] might be soon after smoke inhalation and most likely before classical manifestations of ALI appear. It also provides evidence to consider protective mechanical ventilation strategies for patients with smoke inhalation injury even before a diagnosis of ALI is made, as their lungs may already be inflamed and susceptible to ventilator-induced lung injury. This is relevant for anesthesiologists, who provide mechanical ventilation for these patients after intubation for airway protection and in the operating room during general anesthesia for burn surgery.

Shimazu *et al.*[51] used the multiple inert gas elimination technique to assess the effect of smoke inhalation on ventilation–perfusion distribution. Although the changes that they reported are qualitatively consistent with ours (*i.e.*, shift of perfusion toward the low ventilation–perfusion component and increased heterogeneity of the perfusion-weighted distribution), there are important differences. In fact, we showed that these changes were already present at 3.5 h, whereas their data suggested that they develop 24–48 h after inhalation. Earlier identification of physiologic changes in our study may reflect increased sensitivity of $^{13}N_2$-saline PET compared with multiple inert gas elimination to assess initial stages of ventilation–perfusion mismatch, given the ability of PET to detect functional heterogeneity that occurs at length scales lower than the voxel level.[29,32] However, the two methods have never been compared directly. This early ventilation–perfusion mismatch could also explain why Willey-Courand *et al.*[28] observed a decrease in $Pa_{O_2}$ starting at 1 h after smoke inhalation despite that shunt increased significantly only at 4 h. In that study,[28] the insult was substantially greater than in ours as 100 breaths of cotton smoke were delivered to both lungs. This could explain why they observed an increase in shunt already at 4 h.

## Conclusion

In a large animal model with pulmonary physiology similar to the human, we combined PET imaging of [$^{18}$F]FDG and $^{13}N_2$ kinetics with compartmental modeling to demonstrate that increased pulmonary glucose metabolic rate, indicative of inflammatory cell activation, and ventilation–perfusion mismatch occur by 4 h after acute smoke inhalation. These findings support that pulmonary inflammation and associated lung dysfunction occur early after smoke inhalation.

## Appendix: Computation of Ventilation-to-Perfusion Ratio Distribution

The theoretical background for this method and its implementation have been described in detail previously.[29,32] After a $^{13}N_2$-saline bolus infusion, $^{13}N_2$ activity at the end of apnea (*i.e.*, plateau activity) is proportional to perfusion to aerated units within the region.[30,31] Therefore, for each voxel of lung, $^{13}N_2$ activity at the end of apnea ($A_0$) was taken as proportional to perfusion to aerated units in the voxel ($\dot{Q}$): $A_0 = \eta \cdot \dot{Q}$.

When breathing is resumed, $^{13}N_2$ is cleared from aerated units by ventilation. Consequently, the $^{13}N_2$ washout kinetics after resumption of breathing were used to compute specific ventilation and ventilation-to-perfusion ratios at the voxel level as previously described.[29,32] Briefly, to account for possible intravoxel ventilation and ventilation–perfusion heterogeneity in the computation of total heterogeneity, each voxel was classified as composed of either a single-ventilating compartment, when the semilogarithmic activity–time washout plot was linear, or two compartments, when the washout was not well described by a single line. In one-compartment voxels, specific alveolar ventilation (*i.e.*, alveolar ventilation per unit of gas volume, $s\dot{V}$) was calculated as the reciprocal of the time constant of the $^{13}N_2$ washout curve: $A(t) = A_0 \cdot e^{-t/\tau}$, where $s\dot{V} = 1/\tau$.

In two-compartment voxels, a fast ($\tau_f$) and a slow ($\tau_s$) time constants were fitted to the activity–time points during $^{13}N_2$ washout. $\tau_s$ was obtained from linear fitting of the last 90 s of washout. $\tau_f$ was obtained from fitting the initial portion of the washout curve after subtraction of the component attributable to the slow compartment. To determine the partition of voxel perfusion between the two compartments, the value of activity obtained by extrapolating the last 90 s of washout back to the beginning of washout (*i.e.*, end of apnea) was taken as proportional to perfusion of the slow ventilating compartment:[29]

$$A_{0_s} = \eta \cdot \dot{Q}_s$$

The difference between total activity at the beginning of washout and that attributable to perfusion of the slow compartment was taken as proportional to perfusion of the fast ventilating compartment:

$$A_{0f} = A_0 - A_{0_s} = \eta \cdot \dot{Q} - \eta \cdot \dot{Q}_s = \eta \cdot \dot{Q}_f$$

In order to quantify ventilation-to-perfusion ratios, we started by computing the ratio between specific ventilation and end-apnea activity for each compartment of each voxel. Accordingly, this ratio for one-compartment voxels corresponded to the $s\dot{V}/A_0$ ratio. In two-compartment voxels, there were two ratios:

$$s\dot{V}_f \Big/ A_{0f} = (1/\tau_f)\Big/A_{0f} \text{ for the fast compartment;}$$

$$s\dot{V}_s \Big/ A_{0_s} = (1/\tau_s)\Big/A_{0_s} \text{ for the slow compartment.}$$

We then calculated a perfusion-weighted mean of these ratios $\left(\overline{\dot{sV}/\dot{Q}}\right)$ over both lungs:[29]

$$\overline{\dot{sV}/\dot{Q}} = \frac{\sum_{i=1}^{N} \dot{Q}_{0_i} \cdot \dot{sV}_i / A_{0_i} + \sum_{j=1}^{M} \dot{Q}_{0f_j} \cdot \dot{sV}_{f_j} / A_{0f_j} + \sum_{j=1}^{M} \dot{Q}_{0s_j} \cdot \dot{sV}_{s_j} / A_{0s_j}}{\sum_{i=1}^{N} \dot{Q}_{0_i} + \sum_{j=1}^{M} \dot{Q}_{0f_j} + \sum_{j=1}^{M} \dot{Q}_{0s_j}}$$

$$= \frac{\sum_{i=1}^{N} A_{0_i} \cdot \dot{sV}_i / A_{0_i} + \sum_{j=1}^{M} A_{0f_j} \cdot \dot{sV}_{f_j} / A_{0f_j} + \sum_{j=1}^{M} A_{0s_j} \cdot \dot{sV}_{s_j} / A_{0s_j}}{\sum_{i=1}^{N} A_{0_i} + \sum_{j=1}^{M} A_{0f_j} + \sum_{j=1}^{M} A_{0s_j}}$$

$$= \frac{\sum_{i=1}^{N} \dot{sV}_i + \sum_{j=1}^{M} \dot{sV}_{f_j} + \sum_{j=1}^{M} \dot{sV}_{s_j}}{\sum_{i=1}^{N} A_{0_i} + \sum_{j=1}^{M} A_{0f_j} + \sum_{j=1}^{M} A_{0s_j}}$$

where $N$ is the total number of one-compartment voxels and $M$ is the total number of two-compartment voxels.

Mean-normalized $\dot{sV}/\dot{Q}$ ratios were then computed by dividing compartmental $\dot{sV}/\dot{Q}$ ratios (*i.e.*, $\dot{sV}_i/A_{0_i}$, $\dot{sV}_{f_j}/A_{0f_j}$, and $\dot{sV}_{s_j}/A_{0s_j}$) by $\overline{\dot{sV}/\dot{Q}}$. These mean-normalized $\dot{sV}/\dot{Q}$ ratios were grouped into 80 bins of equal base 10 logarithmic width (0.05) ranging from –2 to 2 and plotted against the corresponding fraction of perfusion in separate distribution histograms for the smoke-exposed and control lungs. These histograms provided mean-normalized distributions of the specific ventilation-to-perfusion ratio. $\dot{sV}/\dot{Q}$ heterogeneity in the smoke-exposed and control lungs was computed as the SD of these perfusion-weighted logarithmic distributions. The rationale for normalizing by a perfusion-weighted mean calculated over both lungs was to allow for comparison of the width and shift of the distribution of the smoke-exposed lung relative to that of the control lung despite the fact that we did not compute ventilation–perfusion distributions in absolute units.

## Acknowledgments

The authors thank Eduardo L. V. Costa, M.D., Ph.D., Research and Education Institute, Hospital Sírio Libanês, São Paulo, Brazil, for assistance with animal experiments; Julian Vasilkoski, B.S., and Lavern E. Keitt, Jr., B.S., Department of Anesthesia, Critical Care, and Pain Medicine, Massachusetts General Hospital and Harvard Medical School, Boston, Massachusetts, for assistance with data analysis.

Supported by a Research Grant 8895, from Shriners Hospitals for Children, Boston, Massachusetts, and by National Institutes of Health Grant R01HL094639, Bethesda, Maryland.

## Competing Interests

The authors declare no competing interests.

## Correspondence

Address correspondence to Dr. Musch: Department of Anesthesia, Critical Care, and Pain Medicine, GRJ-4–418, Massachusetts General Hospital, 55 Fruit Street, Boston, Massachusetts 02114. gmusch@partners.org. 

## References

1. Palmieri TL: Inhalation injury: Research progress and needs. J Burn Care Res 2007; 28:549–54
2. Traber DL, Hawkins HK, Enkhbaatar P, Cox RA, Schmalstieg FC, Zwischenberger JB, Traber LD: The role of the bronchial circulation in the acute lung injury resulting from burn and smoke inhalation. Pulm Pharmacol Ther 2007; 20:163–6
3. American Burn Association: Inhalation injury: Diagnosis. J Am Coll Surg 2003; 196:308–12
4. Edelman DA, White MT, Tyburski JG, Wilson RF: Factors affecting prognosis of inhalation injury. J Burn Care Res 2006; 27:848–53
5. Colohan SM: Predicting prognosis in thermal burns with associated inhalational injury: A systematic review of prognostic factors in adult burn victims. J Burn Care Res 2010; 31:529–39
6. Suzuki M, Aikawa N, Kobayashi K, Higuchi R: Prognostic implications of inhalation injury in burn patients in Tokyo. Burns 2005; 31:331–6
7. Mosier MJ, Pham TN, Park DR, Simmons J, Klein MB, Gibran NS: Predictive value of bronchoscopy in assessing the severity of inhalation injury. J Burn Care Res 2012; 33:65–73
8. Luce EA, Su CT, Hoopes JE: Alveolar-arterial oxygen gradient in the burn patient. J Trauma 1976; 16:212–7
9. Jones WG, Barie PS, Madden M, Finkelstein J, Goodwin CW: The use of compliance in predicting early mortality after inhalation injury. Curr Surg 1988; 45:309–12
10. Tasaki O, Mozingo DW, Dubick MA, Goodwin CW, Yantis LD, Pruitt BA Jr: Effects of heparin and lisofylline on pulmonary function after smoke inhalation injury in an ovine model. Crit Care Med 2002; 30:637–43
11. Abdi S, Herndon D, McGuire J, Traber L, Traber DL: Time course of alterations in lung lymph and bronchial blood flows after inhalation injury. J Burn Care Rehabil 1990; 11:510–5
12. Soejima K, McGuire R, Snyder N IV, Uchida T, Szabó C, Salzman A, Traber LD, Traber DL: The effect of inducible nitric oxide synthase (iNOS) inhibition on smoke inhalation injury in sheep. Shock 2000; 13:261–6
13. Sakurai H, Soejima K, Nozaki M, Traber LD, Traber DL: Effect of ablated airway blood flow on systemic and pulmonary microvascular permeability after smoke inhalation in sheep. Burns 2007; 33:885–91
14. Linares HA, Herndon DN, Traber DL: Sequence of morphologic events in experimental smoke inhalation. J Burn Care Rehabil 1989; 10:27–37
15. Cox RA, Burke AS, Jacob S, Oliveras G, Murakami K, Shimoda K, Enkhbaatar P, Traber LD, Herndon DN, Traber DL, Hawkins HK: Activated nuclear factor kappa B and airway inflammation after smoke inhalation and burn injury in sheep. J Burn Care Res 2009; 30:489–98
16. Hansson L, Ohlsson T, Valind S, Sandell A, Luts A, Jeppsson B, Wollmer P: Glucose utilisation in the lungs of septic rats. Eur J Nucl Med 1999; 26:1340–4
17. Chen DL, Schuster DP: Positron emission tomography with [$^{18}$F]fluorodeoxyglucose to evaluate neutrophil kinetics during acute lung injury. Am J Physiol Lung Cell Mol Physiol 2004; 286:L834–40
18. Chen DL, Rosenbluth DB, Mintun MA, Schuster DP: FDG-PET imaging of pulmonary inflammation in healthy volunteers

after airway instillation of endotoxin. J Appl Physiol 2006; 100:1602–9

19. Musch G, Venegas JG, Bellani G, Winkler T, Schroeder T, Petersen B, Harris RS, Melo MF: Regional gas exchange and cellular metabolic activity in ventilator-induced lung injury. Anesthesiology 2007; 106:723–35
20. Costa EL, Musch G, Winkler T, Schroeder T, Harris RS, Jones HA, Venegas JG, Vidal Melo MF: Mild endotoxemia during mechanical ventilation produces spatially heterogeneous pulmonary neutrophilic inflammation in sheep. Anesthesiology 2010; 112:658–69
21. de Prost N, Costa EL, Wellman T, Musch G, Winkler T, Tucci MR, Harris RS, Venegas JG, Vidal Melo MF: Effects of surfactant depletion on regional pulmonary metabolic activity during mechanical ventilation. J Appl Physiol 2011; 111:1249–58
22. Jones HA, Schofield JB, Krausz T, Boobis AR, Haslett C: Pulmonary fibrosis correlates with duration of tissue neutrophil activation. Am J Respir Crit Care Med 1998; 158:620–8
23. Jones HA, Clark RJ, Rhodes CG, Schofield JB, Krausz T, Haslett C: *In vivo* measurement of neutrophil activity in experimental lung inflammation. Am J Respir Crit Care Med 1994; 149:1635–9
24. Schroeder T, Vidal Melo MF, Musch G, Harris RS, Winkler T, Venegas JG: PET imaging of regional $^{18}$F-FDG uptake and lung function after cigarette smoke inhalation. J Nucl Med 2007; 48:413–9
25. Kikuchi Y, Traber LD, Herndon DN, Traber DL: Unilateral smoke inhalation in sheep: Effect on left lung lymph flow with right lung injury. Am J Physiol 1996; 271(6 Pt 2):R1620–4
26. Westphal M, Cox RA, Traber LD, Morita N, Enkhbaatar P, Schmalstieg FC, Hawkins HK, Maybauer DM, Maybauer MO, Murakami K, Burke AS, Westphal-Varghese BB, Rudloff HE, Salsbury JR, Jodoin JM, Lee S, Traber DL: Combined burn and smoke inhalation injury impairs ovine hypoxic pulmonary vasoconstriction. Crit Care Med 2006; 34:1428–36
27. Ballard-Croft C, Sumpter LR, Broaddus R, Alexander J, Wang D, Zwischenberger JB: Ovine smoke/burn ARDS model: A new ventilator-controlled smoke delivery system. J Surg Res 2010; 164:e155–62
28. Willey-Courand DB, Harris RS, Galletti GG, Hales CA, Fischman A, Venegas JG: Alterations in regional ventilation, perfusion, and shunt after smoke inhalation measured by PET. J Appl Physiol 2002; 93:1115–22
29. Vidal Melo MF, Layfield D, Harris RS, O'Neill K, Musch G, Richter T, Winkler T, Fischman AJ, Venegas JG: Quantification of regional ventilation-perfusion ratios with PET. J Nucl Med 2003; 44:1982–91
30. Musch G, Harris RS, Vidal Melo MF, O'Neill KR, Layfield JD, Winkler T, Venegas JG: Mechanism by which a sustained inflation can worsen oxygenation in acute lung injury. Anesthesiology 2004; 100:323–30
31. Galletti GG, Venegas JG: Tracer kinetic model of regional pulmonary function using positron emission tomography. J Appl Physiol 2002; 93:1104–14
32. Melo MF, Harris RS, Layfield JD, Venegas JG: Topographic basis of bimodal ventilation-perfusion distributions during bronchoconstriction in sheep. Am J Respir Crit Care Med 2005; 171:714–21
33. Schroeder T, Vidal Melo MF, Musch G, Harris RS, Venegas JG, Winkler T: Image-derived input function for assessment of $^{18}$F-FDG uptake by the inflamed lung. J Nucl Med 2007; 48:1889–96
34. Sokoloff L, Reivich M, Kennedy C, Des Rosiers MH, Patlak CS, Pettigrew KD, Sakurada O, Shinohara M: The [14C]deoxyglucose method for the measurement of local cerebral glucose utilization: Theory, procedure, and normal values in the conscious and anesthetized albino rat. J Neurochem 1977; 28:897–916
35. Phelps ME, Huang SC, Hoffman EJ, Selin C, Sokoloff L, Kuhl DE: Tomographic measurement of local cerebral glucose metabolic rate in humans with (F-18)2-fluoro-2-deoxy-D-glucose: Validation of method. Ann Neurol 1979; 6:371–88
36. Armitage P, Berry G: Chapter 13: Distribution-free methods, Statistical Methods in Medical Research, 2nd edition. Oxford, Blackwell Scientific Publications, 1987, pp 409–10
37. Till GO, Hatherill JR, Tourtellotte WW, Lutz MJ, Ward PA: Lipid peroxidation and acute lung injury after thermal trauma to skin. Evidence of a role for hydroxyl radical. Am J Pathol 1985; 119:376–84
38. Soejima K, Schmalstieg FC, Sakurai H, Traber LD, Traber DL: Pathophysiological analysis of combined burn and smoke inhalation injuries in sheep. Am J Physiol Lung Cell Mol Physiol 2001; 280:L1233–41
39. Deichen JT, Prante O, Gack M, Schmiedehausen K, Kuwert T: Uptake of [$^{18}$F]fluorodeoxyglucose in human monocyte-macrophages *in vitro*. Eur J Nucl Med Mol Imaging 2003; 30:267–73
40. Harris RS, Venegas JG, Wongviriyawong C, Winkler T, Kone M, Musch G, Vidal Melo MF, de Prost N, Hamilos DL, Afshar R, Cho J, Luster AD, Medoff BD: $^{18}$F-FDG uptake rate is a biomarker of eosinophilic inflammation and airway response in asthma. J Nucl Med 2011; 52:1713–20
41. Maschauer S, Prante O, Hoffmann M, Deichen JT, Kuwert T: Characterization of $^{18}$F-FDG uptake in human endothelial cells *in vitro*. J Nucl Med 2004; 45:455–60
42. Saha D, Takahashi K, de Prost N, Winkler T, Pinilla-Vera M, Baron RM, Vidal Melo MF: Micro-autoradiographic assessment of cell types contributing to 2-deoxy-2-[$^{18}$F]fluoro-D-glucose uptake during ventilator-induced and endotoxemic lung injury. Mol Imaging Biol 2013; 15:19–27
43. Chen DL, Bedient TJ, Kozlowski J, Rosenbluth DB, Isakow W, Ferkol TW, Thomas B, Mintun MA, Schuster DP, Walter MJ: [$^{18}$F]fluorodeoxyglucose positron emission tomography for lung antiinflammatory response evaluation. Am J Respir Crit Care Med 2009; 180:533–9
44. Oh JS, Chung KK, Allen A, Batchinsky AI, Huzar T, King BT, Wolf SE, Sjulin T, Cancio LC: Admission chest CT complements fiberoptic bronchoscopy in prediction of adverse outcomes in thermally injured patients. J Burn Care Res 2012; 33:532–8
45. Torizuka T, Tamaki N, Inokuma T, Magata Y, Sasayama S, Yonekura Y, Tanaka A, Yamaoka Y, Yamamoto K, Konishi J: *In vivo* assessment of glucose metabolism in hepatocellular carcinoma with FDG-PET. J Nucl Med 1995; 36:1811–7
46. Wahl RL, Zasadny K, Helvie M, Hutchins GD, Weber B, Cody R: Metabolic monitoring of breast cancer chemohormonotherapy using positron emission tomography: Initial evaluation. J Clin Oncol 1993; 11:2101–11
47. Perng DW, Chang TM, Wang JY, Lee CC, Lu SH, Shyue SK, Lee TS, Kou YR: Inflammatory role of AMP-activated protein kinase signaling in an experimental model of toxic smoke inhalation injury. Crit Care Med 2013; 41:120–32
48. Rehberg S, Enkhbaatar P, Traber DL: AMP-activated protein kinase signaling pathway in toxic smoke inhalation injury: Nice to demonstrate, nice to know, but is there a therapeutic relevance? Crit Care Med 2013; 41:349–50
49. Hamahata A, Enkhbaatar P, Lange M, Yamaki T, Nakazawa H, Nozaki M, Sakurai H, Traber LD, Traber DL: Administration of a peroxynitrite decomposition catalyst into the bronchial artery attenuates pulmonary dysfunction after smoke inhalation and burn injury in sheep. Shock 2012; 38:543–8
50. Hamahata A, Enkhbaatar P, Lange M, Yamaki T, Sakurai H, Shimoda K, Nakazawa H, Traber LD, Traber DL: Administration of poly(ADP-ribose) polymerase inhibitor into bronchial artery attenuates pulmonary pathophysiology after smoke inhalation and burn in an ovine model. Burns 2012; 38:1210–5

51. Shimazu T, Yukioka T, Ikeuchi H, Mason AD Jr, Wagner PD, Pruitt BA Jr: Ventilation-perfusion alterations after smoke inhalation injury in an ovine model. J Appl Physiol 1996; 81:2250–9
52. Enkhbaatar P, Wang J, Saunders F, Lange M, Hamahata A, Rehberg S, Parkinson JF, Traber LD, Herndon DN, Traber DL: Mechanistic aspects of inducible nitric oxide synthase-induced lung injury in burn trauma. Burns 2011; 37:638–45
53. Lange M, Szabo C, Enkhbaatar P, Connelly R, Horvath E, Hamahata A, Cox RA, Esechie A, Nakano Y, Traber LD, Herndon DN, Traber DL: Beneficial pulmonary effects of a metalloporphyrinic peroxynitrite decomposition catalyst in burn and smoke inhalation injury. Am J Physiol Lung Cell Mol Physiol 2011; 300:L167–75
54. Laffon M, Pittet JF, Modelska K, Matthay MA, Young DM: Interleukin-8 mediates injury from smoke inhalation to both the lung endothelial and the alveolar epithelial barriers in rabbits. Am J Respir Crit Care Med 1999; 160(5 Pt 1): 1443–9
55. Efimova O, Volokhov AB, Iliaifar S, Hales CA: Ligation of the bronchial artery in sheep attenuates early pulmonary changes following exposure to smoke. J Appl Physiol 2000; 88:888–93
56. Katahira J, Murakami K, Schmalstieg FC, Cox R, Hawkins H, Traber LD, Traber DL: Role of anti-L-selectin antibody in burn and smoke inhalation injury in sheep. Am J Physiol Lung Cell Mol Physiol 2002; 283:L1043–50
57. Ischiropoulos H, Mendiguren I, Fisher D, Fisher AB, Thom SR: Role of neutrophils and nitric oxide in lung alveolar injury from smoke inhalation. Am J Respir Crit Care Med 1994; 150:337–41
58. Thai A, Xiao J, Ammit AJ, Rohanizadeh R: Development of inhalable formulations of anti-inflammatory drugs to potentially treat smoke inhalation injury in burn victims. Int J Pharm 2010; 389:41–52